Neutron and beta imaging with Micromegas detectors with optical readout

A. Cools, S. Aune, F. Beau, M. Benali, F.M. Brunbauer, T. Benoit, D. Desforge, E. Ferrer-Ribas, C. Malgorn, E. Oliveri, et al.

Neutron and beta imaging with Micromegas detectors with optical readout

A. Cools[a], S. Aune[a], F. Beau[b], M. Benali[c], F.M. Brunbauer[d], T. Benoit[a], D. Desforge[a], E. Ferrer-Ribas[a], C. Malgorn[b], E. Oliveri[d], T. Papaevangelou[a], E. C. Pollacco[a], L. Ropelewski[d], A. Sari[c]

a IRFU, CEA, Université Paris-Saclay, F-91191 Gif-sur-Yvette, France
b Institut Joliot, CEA, Université Paris-Saclay, F-91191 Gif-sur-Yvette, France
c LIST, CEA, Université Paris-Saclay, F-91191 Gif-sur-Yvette, France
d European Organization for Nuclear Research (CERN), 1211 Geneva 23, Switzerland

Abstract

Recent developments have shown that coupling a Micromegas gaseous detector on a glass substrate with a transparent anode and a CMOS camera enables the optical readout of Micromegas detectors with a good spatial resolution, demonstrating that the glass Micromegas detector is well-suited for imaging. This feasibility test has been effectuated with low-energy X-ray photons also permitting energy resolved imaging. This test opens the way to different applications. Here we will focus on two applications. Namely, neutron imaging for non-destructive examination of highly gamma-ray emitting objects, such as irradiated nuclear fuel or radioactive waste. And secondly, we are developing a beta imager for the cell tagging in the field of anticancerous drug studies.

Both applications require to design the detectors in view of the specific constraints of reactor dismantling and medical applications: spatial resolution and strong gamma suppression for neutron imaging and precise rate and energy spectrum measurements for the beta.

A dedicated system consisting of a glass Micromegas detector and an ultrasensitive camera has been designed and assembled. Here we present the first results from the characterization of the detectors, as well as the first acquired images.

Keywords

Micromegas, Glass Micromegas, Gaseous detector, Optical readout, MPGD, Beta imager, Neutron radiography

1. Introduction

Charge-readout Micromegas are widely used in high energy physics, nuclear physics and societal applications [1]. On the other hand, several types of gaseous detectors were proved to be suitable for optical readout, such as Time Projection Chambers (TPCs) [2] for 3D track reconstruction or Gaseous Electron Multipliers (GEMs). Previous works have shown that the GEM multilayer foils structure allows very high gain and sufficient scintillation light yield for efficient readout [3]. Recent developments [4] have shown that coupling a Micromegas gaseous detector with a transparent glass anode and a sensitive CCD or CMOS camera enables the optical readout of the detector with a good spatial resolution, demonstrating that the glass Micromegas is well-suited for imaging applications.

The optical readout Micromegas detector allows to take advantage of the Micromegas high gain and can be accompanied by an important scintillation light yield when an appropriate gas mixture is used. On the other hand, CMOS cameras offer mega pixel resolution with single photon detection capability, which makes optical readout Micromegas suitable for imaging of a wide variety of sources, with different energies and intensities. In addition, optical readout Micromegas offers the possibility to integrate the light in every pixel for long integration time and to perform real-time imaging without heavy data processing.

Classical Micromegas detectors are integrated on opaque substrates such as Printed Circuit Boards (PCBs) which thwart the optical readout process. This new detector is implemented on a glass substrate covered by a thin layer of Indium Tin Oxide (ITO) depicting the anode. A micromesh is supported by insulating pillars regularly distributed on the anode to ensure a constant amplification gap between the mesh and the anode (Fig. 1). The detector is filled with Argon and Carbon tetrafluoride (CF_4) gas mixture which scintillates in ultraviolet (UV), visible (VIS) and near infrared (NIR) wavelength ranges with a wide emission band in the visible [5]. The VIS

emission band matches the wavelengths where ITO has a maximum transparency and the CCD and CMOS imaging sensors have important quantum efficiency (QE).

In this paper, we present two on-going glass Micromegas applications: neutron radiography and β-imaging. Neutron radiography represents a very powerful tool for reactor material testing and non-destructive examination of nuclear fuel or radioactive waste in a very high γ-flux environment. The goal of this device is to perform real-time neutron radiography with a spatial resolution of the order of hundreds of µm and gamma rejection of the order of 10^{-8} in a 10^{6} s^{-1} cm^{-2} neutron flux. This level of gamma rejection has already been demonstrated with charge readout Micromegas [6]. The Micromegas was equipped with a cathode with a thin (1.5 µm) $^{10}B_4C$ deposition converting low-energy neutrons to α or ^{7}Li particles, which then ionize the gas. The much higher ionization power of those particles compared to electrons, allows the strong suppression of γ signals using only the pulse amplitude information.

The second glass Micromegas application aims to measure single tumour cells drug concentration in order to study cancer treatment drugs efficiency. Radio-labelling allows to assess the behavior and biodistribution of drugs in a context of pharmaceutical studies. For precise quantification of drug and conservation of the drug chemistry and metabolism, ^{3}H and ^{14}C are ideal radio-labelling candidates. Moreover, single-cell level quantification of drug has become a critical matter in oncology since cell heterogeneity was discovered decades ago [7]. This emphasizes the need of developing a β-imager detector able to measure sub-becquerel activities from single cells tracked with ^{3}H. Recent studies have shown that Micromegas detectors are well suited for the imaging of sub-becquerel β emitting trackers [8]. Coupling a Micromegas detector with an optical readout provides measurement of very low activity thanks to the Micromegas detector high efficiency and low energy threshold while profiting from the high spatial resolution of imaging sensor and real-time imaging capacity.

2. Detector description

In this section, the glass Micromegas detector mechanics, the chosen gas mixture and the optical system are depicted.

2.1. The glass Micromegas

The main feature of the glass Micromegas detector is that the anode is made of a transparent glass coated with a layer of ITO. Two types of anode were used: one thin anode of 1.1 mm of regular glass and one thick anode of 5 mm of pure quartz with better transparency. The ITO deposit is made with a thickness of 150 (±10) nm with a resistivity of about 100Ω for the whole surface. The mesh is integrated using the 'bulk' process [1] with a woven stainless-steel mesh (45 µm aperture and 18 µm wire) and 600 µm diameter pillars of Pyralux with a 6 mm minimum distance between pillars and a hexagonal shape for active area maximization (Fig. 1 left). Up to now, all detectors have an active area of 8x8 cm^2. In a 'bulk' Micromegas, the mesh is encapsulated in the pillar so that the mesh, the pillars and the anode constitute one entity. On Fig. 2, the amplification gap is defined between the coated anode (glass anode + ITO) and the mesh (dotted line). PCBs (Fig. 1 right) are used to define the drift gap (few mm width depending on the application) between the mesh and the cathode (solid line in Fig. 2). The cathode is made of a 20 µm thickness Mylar foil coated with aluminum, stretched on a solid aluminum frame. In order that electrons drift towards the mesh and that they are amplified on the amplification gap, negative voltages are applied both on the cathode and the mesh and the anode is grounded. Since only the material of the anode is different, the intrinsic properties of the Micromegas remains the same as a classical 'bulk' Micromegas.

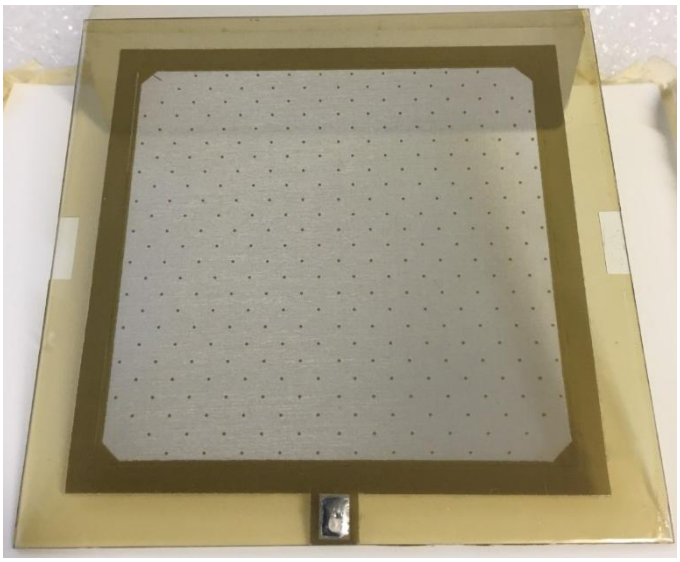

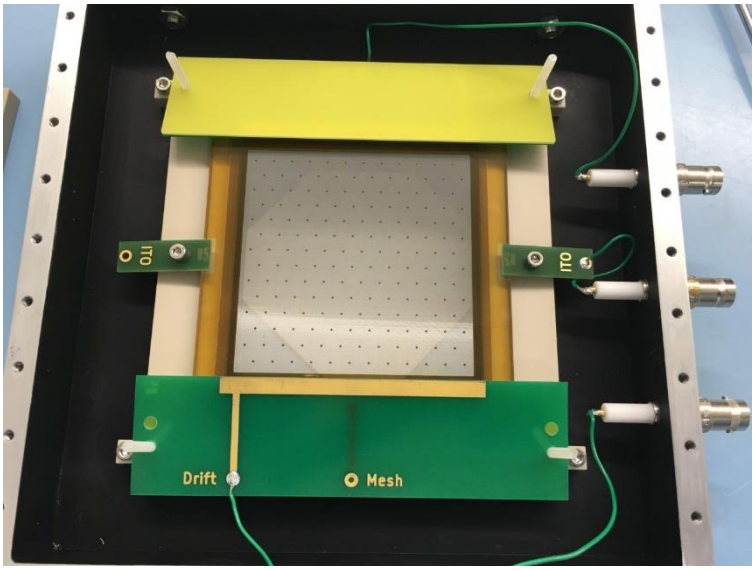

Fig. 1. Photos of the detector. Left: Transparent glass bulk Micromegas. Right: Detector's mechanics with electrical signal ensured by pressure connectors in PCB.

2.2. Gas mixture choice

The gas mixture is composed of 80% of argon and 20% of CF_4. There are two different light emission mechanisms that occur in such gas mixture: phosphorescence and fluorescence. Phosphorescence has a very long signal response to first excitation of the gas molecules from 100 ms to 100 sec whereas fluorescence is a very prompt emission of light from 1 ns to 1 µs. Hence, the fluorescence mechanism is more important since the light emission is synchronized with particle interaction with the gas.

In a Micromegas detector, there are two steps of electron production: the primary electrons coming from the excitation of the gas due to incident particles interactions in the drift gap and the secondary electrons from the avalanche amplification in the amplification gap. Similarly, primary scintillation occurs during primary electrons production and secondary scintillation during avalanche multiplication with a very large amount of light production (Fig. 2).

The amount of light created during these processes is defined by the light yield, which depends on the electric fields, the pressure of the gas and the gas mixture. CF_4 based gas mixtures are able to reach a light yield of 0.1 to 0.3 secondary scintillation photons per secondary electron [9] in avalanche multiplication with a gain over 10^4.

According to [3], the gas mixture with 20% of CF_4 shows a better light yield than the other Ar/CF_4 gas mixtures. Moreover, $Ar+CF_4$ gas mixture emits in UV, visible and near infrared wavelengths with a wide wavelength band in the visible peaking at 630 nm [5]. At 630 nm wavelength, ITO has a transparency of 80% [4] which also corresponds to the maximum QE of our CMOS sensor of about 70% (Fig. 3) [10]. This light emission in the VIS mainly comes from CF_3^* de-excitation, which is produced by CF_4^* dissociation and electron impact mechanisms.

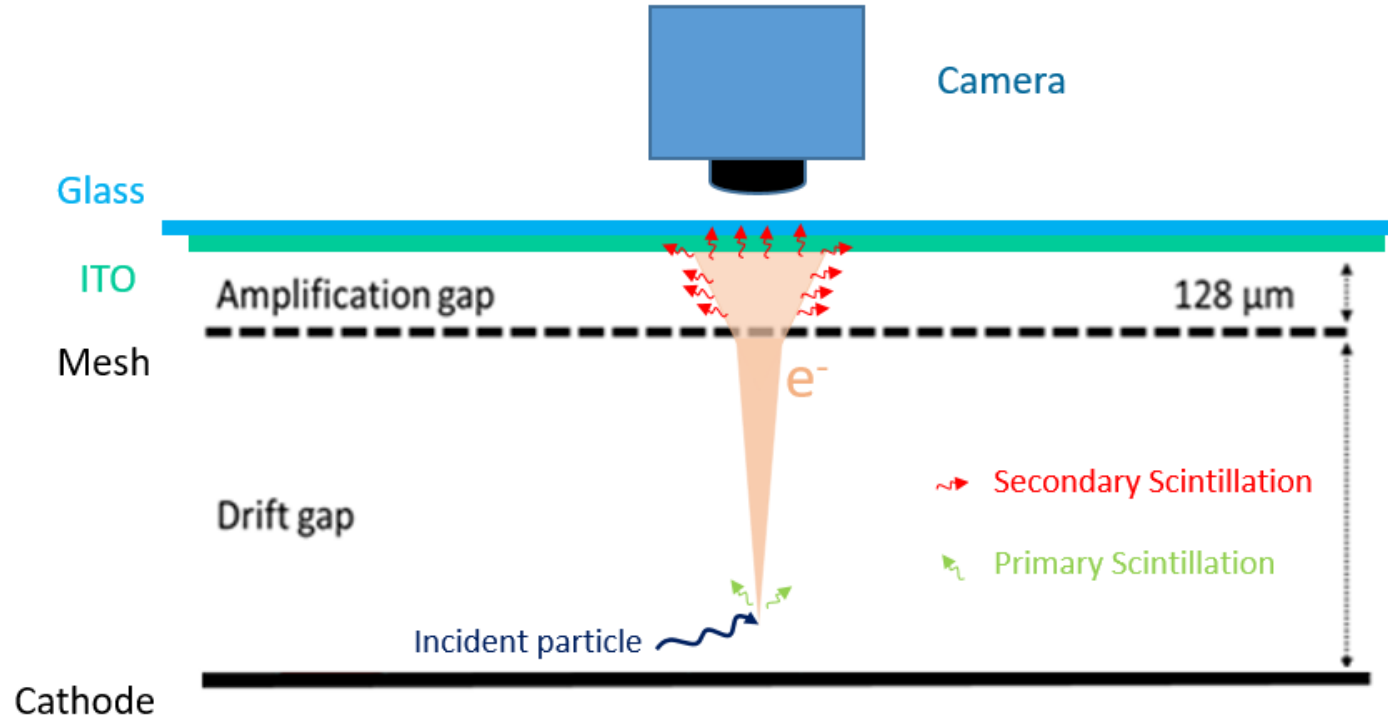

Fig. 2. Sketch of the glass Micromegas with process description. The bulk Micromegas is implemented on a glass anode coated with ITO.

2.3. Imaging sensor

The Micromegas detector is coupled with a light detection device in order to read out the visible light. CMOS sensor is a first rate choice because of its very low readout noise. The imaging sensor is an ORCA-Quest qCMOS camera from Hamamatsu [10] which is capable of single photon detection. In fact, this camera is able to reach a readout noise of 0.27 e^- RMS in "ultra quiet" mode with a dark current of 0.006 e^-/pixel/s. It has a 10 Hz acquisition rate in quiet mode and a 120 Hz rate in standard mode when increasing the readout noise to 0.43 e^- RMS. Its 8 megapixel resolution combined with the extreme low noise makes this camera very suitable for low energy particle imaging and neutron radiography. The camera is combined with a 25 mm lens of f/0.95 aperture and large sensor size from Schneider Optics capable of low light quantity imaging.

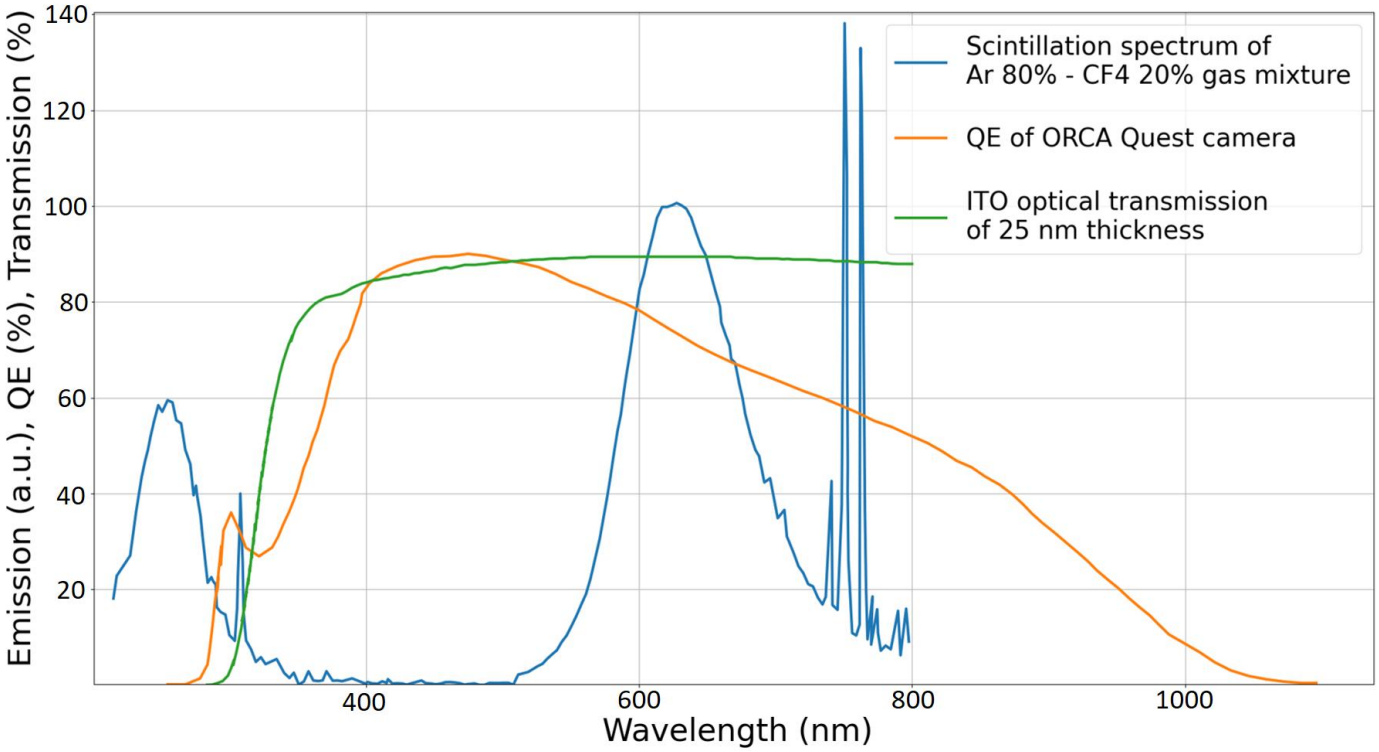

Fig. 3. QE of the ORCA Quest camera reaching 70% at 630 nm. Ar/CF4 gas mixture scintillation spectrum normalized to the wavelength band peaking at 630 nm. ITO optical transmission for a film of ITO of 25 nm thickness. The transmission is at 80% in the visible. Adapted from [4,10].

3. X-ray characterization

Making a Micromegas detector on a glass substrate involves many challenges regarding the mechanical weakness of the glass. In fact, using a thin glass substrate, the glass might break under the pressure from the stretching of the mesh. The tension applied on the mesh is kept between 5 and 15 Newtons/cm depending on the thickness of the glass to minimize the tension applied on the glass. The deformation of the glass influences the quality of the amplification gap and has consequences on the energy resolution, homogeneity of the gain and sparking point of the detector. For this reason, we characterize the detector with an X-ray ^{55}Fe source. In this setup, the detector mechanics is made of an aluminum foil front window and the cathode is a thin aluminized Mylar film to be transparent to 5.9 keV ^{55}Fe X-rays source.

X-rays sources were used for different purposes: first, the charge readout mode was used for gain and energy resolution characterization, then optical readout for gain homogeneity, contrast and spatial resolution data collection.

3.1. Gain and energy resolution characterization using the charge readout mode

The energy resolution was measured with charge readout in Argon + 20% CF_4 gas mixture using a ^{55}Fe source. To measure the charge signal from the mesh, an ORTEC preamplifier and amplifier and an Amptek MultiChannel Analyzer (MCA) were used in series. A fit of the sum of two Gaussian functions was applied on the ^{55}Fe spectrum around 5.9 keV. A 14% energy resolution and a gain above 10^4 were assessed for one of the first glass Micromegas made at CEA (Fig. 4).

3.2. X-ray beam characterization with optical readout

In a second phase, homogeneity of the gain, contrast of the image and spatial resolution were evaluated with a higher flux X-ray source from an X-ray tube at the Gas Detector Development (GDD) group at CERN. At a voltage of 20 kV and a current of about 100 µA, the generator creates X-rays with a continuous energy spectrum peaking at 8 keV at high flux. To perform X-ray radiography, the scintillation light is optically read out by recording the integrated light intensity of every pixels. By placing the X-ray tube 1m away from the generator, a rather flat beam profile is obtained. In Fig. 5, the detector signal across the full active area is displayed. It shows a uniform response of the signal with a Gaussian profile which corresponds to the X-ray tube beam profile. Pillars behave as dead zones and appear as dark dots. In this configuration, the anode voltage is at 550 V with a

128 µm amplification gap, the cathode is set at -100 V with a 2 mm drift gap and the mesh is grounded. A single image of 60 sec exposure time was acquired, from which we subtracted a background image taken with no voltage, no X-rays and with the same exposure time.

Following this, an object is placed in front of the detector for radiography images. The body of a bat was put on the front windows of the detector, giving the image shown on Fig. 6. The image is corrected by dividing it by the previous flat image taken without any object in front. Then, the beam profile is flattened and the contrast is increased. Here, the internal structure of the bat is clearly depicted and small details like the finger bones are visible. This points out the optical readout method potential to acquire easily highly resolved and contrasted images.

3.3. Next steps: spatial resolution measurement with a lead pattern.

X-ray radiography allows to calculate the device spatial resolution by using a lead target with patterns of different spatial frequencies. The target is placed inside the gas volume as close as possible to the cathode. This way the parallax effect coming from the non parallel X-rays tracks is minimized. As shown on Fig. 7, each pattern of the target corresponds to a spatial frequency and will lead to a Modulation Transfer Function (MTF) measurement of the device. Ongoing analysis aims to measure the contrast for each pattern of the target towards MTF study.

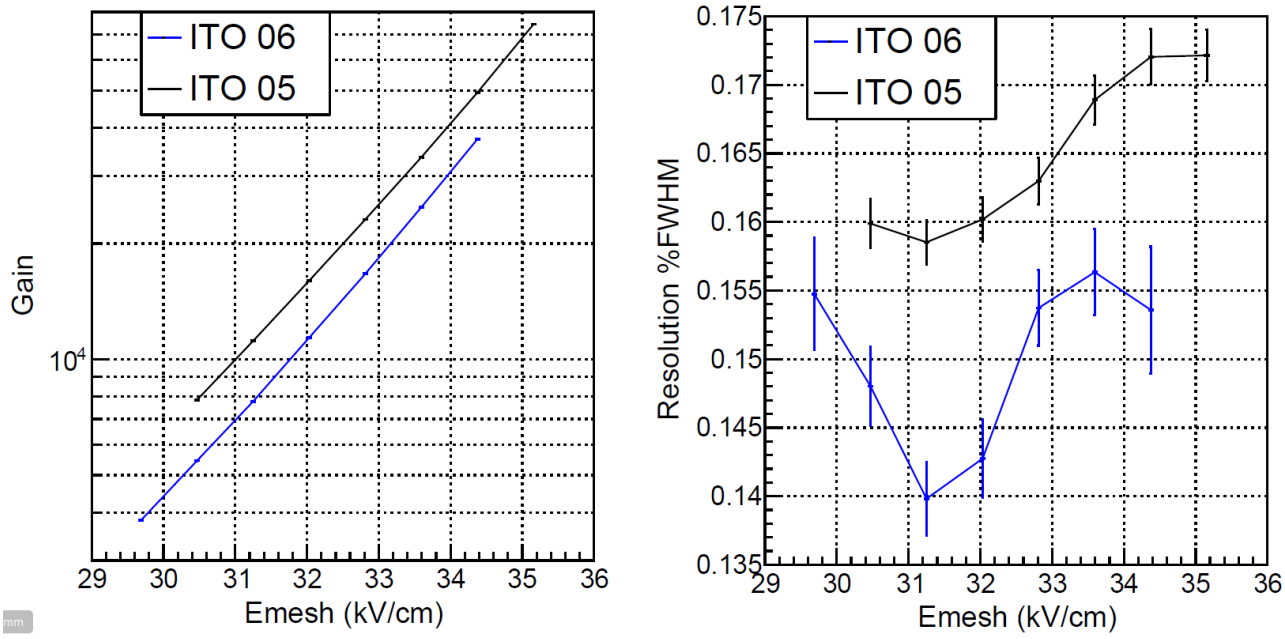

Fig. 4. Left: Gain versus amplification field for two glass Micromegas detectors. Right: Energy Resolution versus amplification.

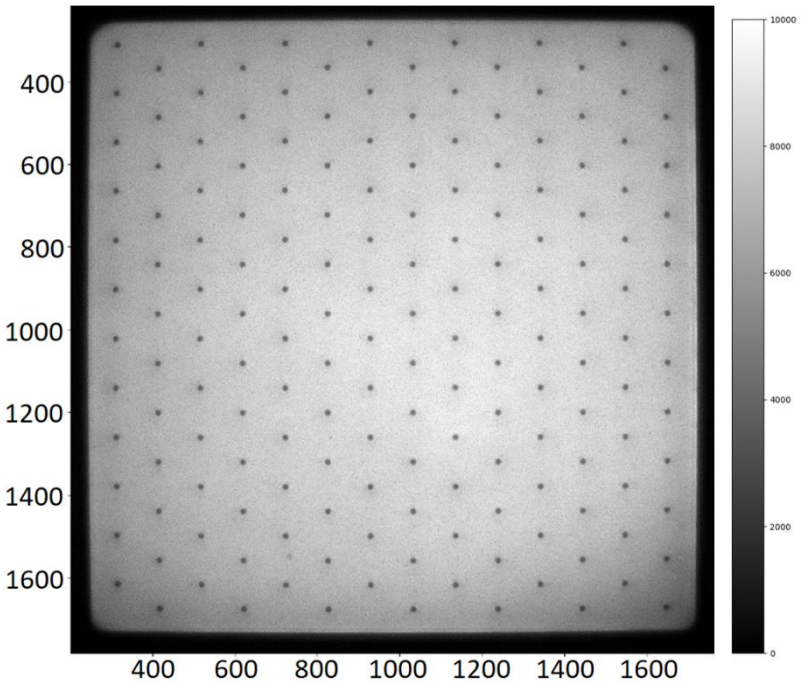

Fig. 5. 60 sec exposure time full active area image of the glass Micromegas detector with simple background suppression.

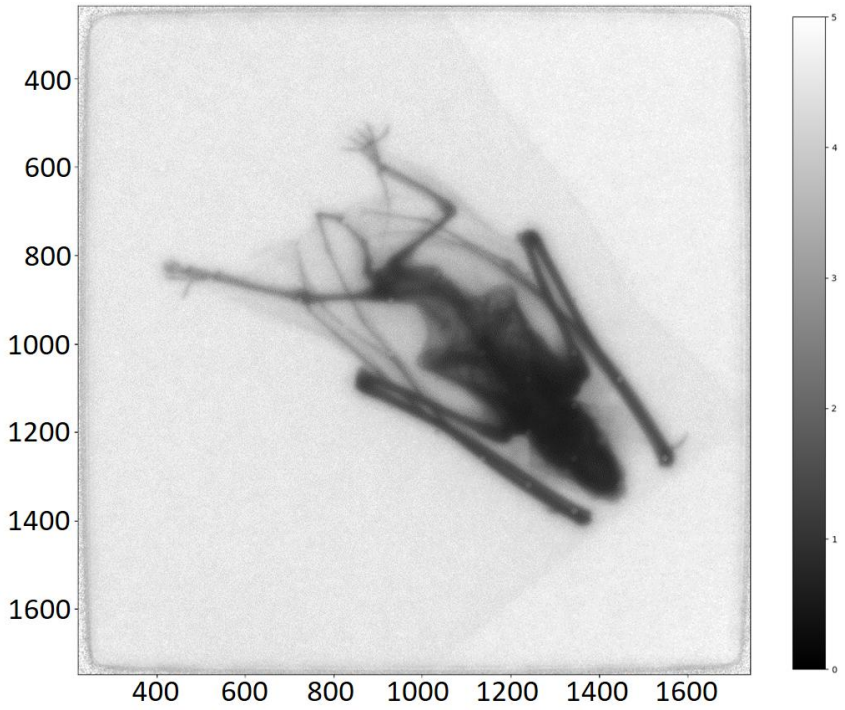

Fig. 6. 60 sec exposure time bat radiography with simple background suppression and beam profile correction. The shadowing from the plastic bag containing the bat is also visible.

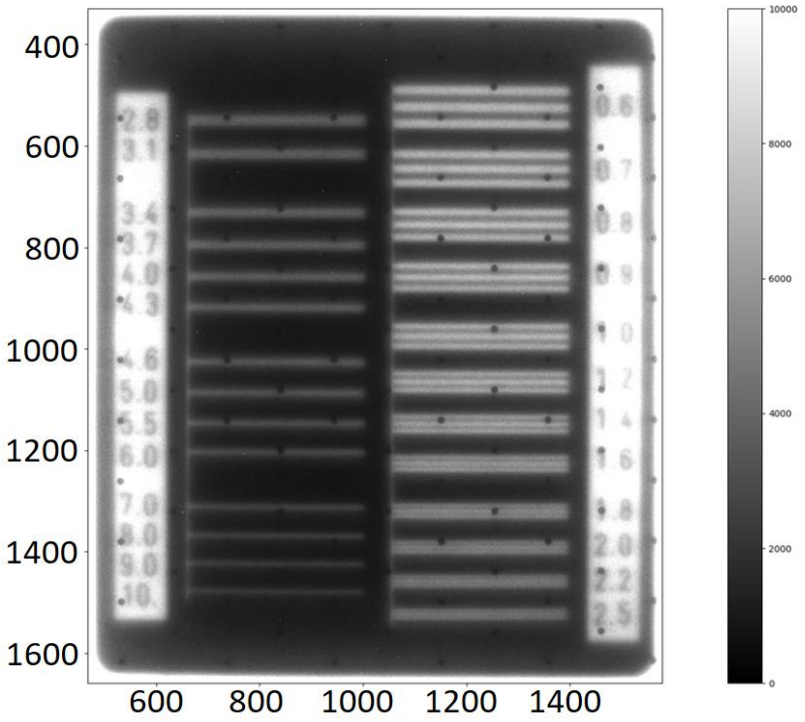

Fig. 7. 60 sec exposure time lead target radiography with simple background suppression. The different frequencies of the patterns correspond to different spatial frequencies.

4. Optical readout applications

Regarding the high suitability of optical readout Micromegas for imaging, we have foreseen two applications for this detector.

For both applications, the optical readout device offers two data taking methods: image integration allows real-time imaging with almost no data treatment whereas event-by-event acquisition leads to track reconstruction resulting to better spatial resolution and stronger γ suppression in the case of neutron radiography.

4.1. Beta imaging at the single cell level

Drug tracking with radionuclide is a major method for cancer drug study, especially when reaching the single cell scale. Tritium (^{3}H) has two more neutrons than hydrogen but behaves very similarly on the chemical aspect. In the biology field, ^{3}H is far more convenient since it substitutes hydrogen and preserves the metabolism of the drug molecule. On the opposite, fluorescence is also a common tool for drug targeting but it involves large molecules with fluorite, which disrupts the drug molecule's structure.

Tritium emits β^- particles with an average energy of 5.7 keV. The activity of a cell labelled with tritium is expected to be below 1 Bq. Hence, the detector has to reach the sub-becquerel activity detection level.

In previous studies, it has been shown that a Micromegas detector with charge readout is capable of measuring tritiated samples in the sub-becquerel activity region [11]. The present goal is to perform the same measurement with optical readout Micromegas taking advantage of the device real-time imaging capability, high spatial resolution and imaging sensor handiness.

4.1.1. Experimental setup

As a first test, tritiated glucose (^{3}H-glucose) was used instead of living tumour cells for convenience. Solutions of ^{3}H-glucose are prepared in a solvent made of 50% distilled water and 50% of ethanol for quicker drying time. Only two activities were chosen : 0.3 Bq and 60 Bq per 1 µL droplet. These activity ranges demonstrate both the detector low activity measurement capacity and its dynamic range in terms of event counting. The samples are inside the gas volume, deposited on the cathode because of the short β particle range in matter (Fig. 8). In fact, β^- particles from tritium have an energy below 14 keV where the particle's range does not exceed 1 mm inside gas [11].

The detector is a 128 µm amplification gap glass Micromegas with a 6 mm drift gap, filled with 20% of CF4 and 80% of Argon. 12 droplets are deposited on the cathode for each activity with a 2 mm, 1 mm and 0.5 mm gap between (Fig. 9 right). The distance between the lens of the camera and the front window of the detector is set at the minimum working distance of the lens (30 cm) to capture as much scintillation light as possible. Two kinds of data were acquired : integrated images with long exposure time frames and event-by-event images with short exposure time.

4.1.2. Integration method

For the integration method, we sum up 180 light intensity images of 10 sec to minimize the dark current noise while getting enough statistic (30 min in total). The background is suppressed by subtracting black images taken without any electric field in the amplification and drift gaps. As we can see on the Fig. 9 on the left, 60 Bq droplets clearly appear and even the 5 mm separated droplets are well distinguishable. However, the 0.3 Bq drops are hardly visible but their positions is identifiable. The specific detector used in this measurement was not optimal so it is not surprising to loose light when looking at the very low activity drops. In fact, the camera suffers by many reflections coming from the inner part of the mechanics, which lowers the Signal-to-Noise Ratio (SNR). Also, some light leaks from the ambient light are still penetrating the gas volume. In the future, a blackened mechanics will be use avoiding any shining effects or light leak.

4.1.2. Event-by-event method

A clustering algorithm was developed for measurement of single event. For event-by-event analysis, 20 000 frames of 100 msec were acquired to avoid the overlap of events and the overall acquisition time is 33 min. For the background subtraction, we perform individual pixel background thresholding: for each pixel, the mean value and standard deviation (σ) over a hundred background images are measured to define a threshold at 2 to 5 values of σ. The Python programming language offers very handy and fast tools to manipulate matrixes of pixels and to apply a threshold to each pixel.

Furthermore, the algorithm identifies the clusters and measures their barycenter to reconstruct the initial position of the glucose sample. On Fig. 10, we can clearly observe both the high and low activity drops with a precise measurement of their position. This plot depicts the histogram of the positions of the clusters as a function of the *x* and *y* axis. When we divide this plot by the overall duration of the acquisition, we access to the activity of each drop. The activity measurement requires more experimental studies to be lead in collaboration with the biologists. Nevertheless, this method demands longer duration (several hours) of data computing compared to the image integration method.

4.1.3. Next steps

Our immediate priority is to obtain a better SNR for low activity measurements with integrated images. Other studies are ongoing to measure single ^{3}H event light intensity with a Photomultiplier tube (PMT). In this way, we will measure the activity of the samples with integrated images by normalizing an image by a single event intensity value. Moreover, we have been working with microfluidics researchers in order to isolate single cell. Soon, we will use blobs of several tritiated cells as samples first and then single cells. For the activity measurement, it is also planned to measure the samples activity in parallel with liquid scintillation counting as a reference. Finally, there will be simulation studies on the β^- particles behavior in the drift gap.

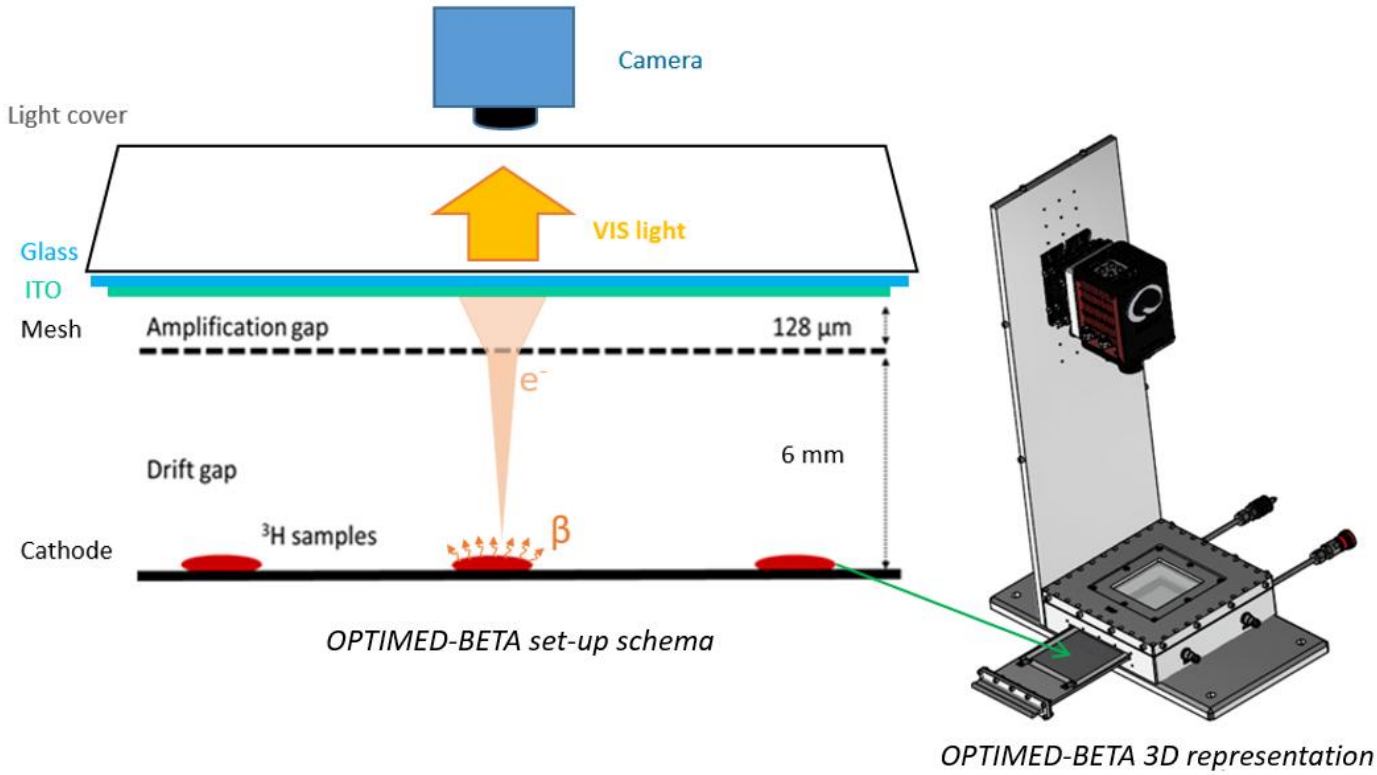

Fig. 8. Sketch of the Optimed-Beta setup. ^{3}H are deposit inside the gas volume on the cathode. Inset: 3D representation of Optimed-Beta setup.

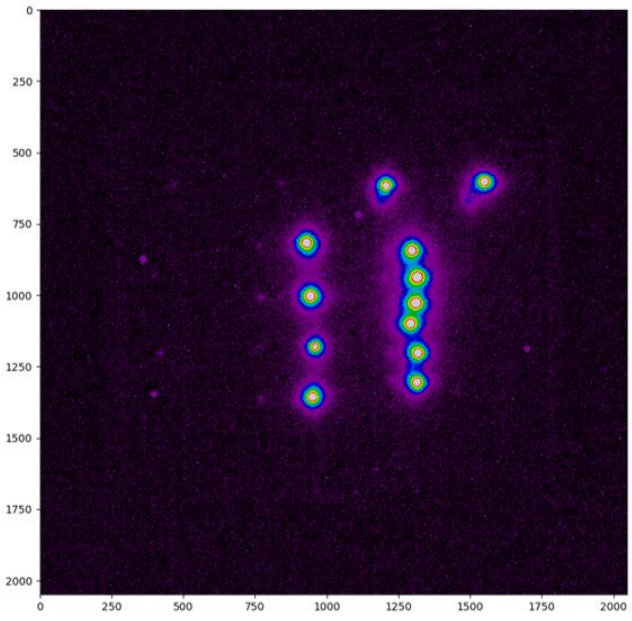

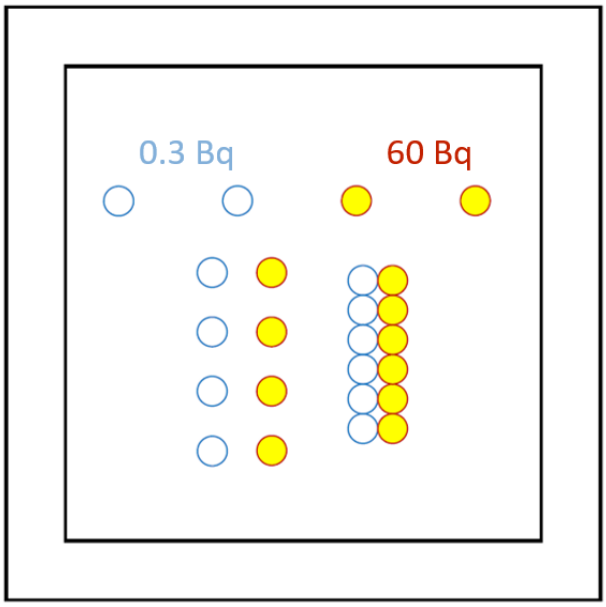

Fig. 9. Left: 180 integrated images of 10 sec showing the light intensity from ^{3}H samples of 0.3 Bq and 60 Bq. Right: Cartoon of the samples positions and activities.

4.2. Neutron radiography

This project aims to develop a neutron radiography system for the SAPHIR platform and for the Jules Horowitz Reactor for nuclear waste and nuclear fuel characterization respectively. In a first step, a prototype of 10x10 cm^2 active area will be tested.

4.2.1. Experimental set-up

This setup requires a neutron-to-charge converter to be placed in the gas volume and on the cathode, as shown on Fig. 11. Here we use a 1.5 µm thick B_4C converter deposited on a copper cathode, giving a ~5% conversion rate for thermal neutrons. In addition, the operation in a high-radiation environment could damage the camera. For this reason, we insert a mirror between the back window of the Micromegas and the camera in order to shield the camera and keep it outside of the neutron beam. The device remains radiation hard since the Micromegas detector can sustain high particle interaction rates up to 10^6 s^{-1} mm^{-2} [1,6].

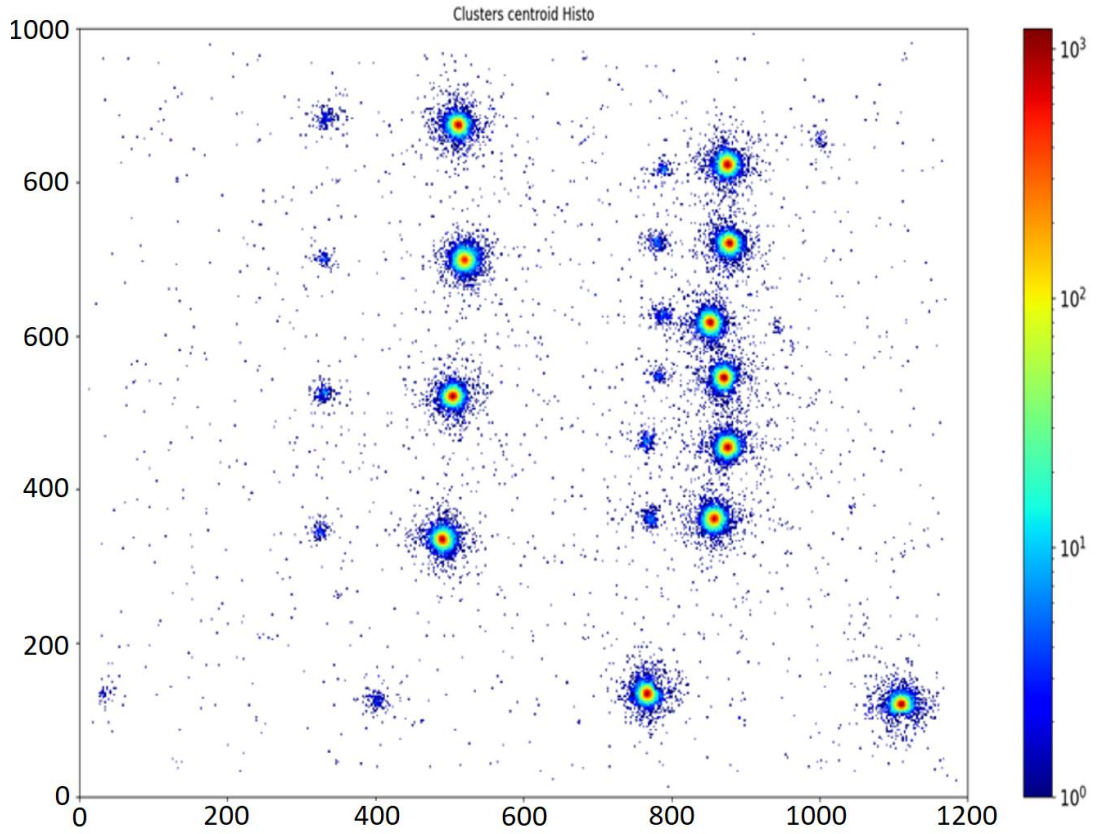

Fig. 10. Histogram of the clusters positions over 20000 images of 100 msec. The barycenter of the events from ^{3}H samples of 0.3 Bq and 60 Bq are calculated. Every samples sketched in Fig. 9 right are localized.

4.2.1. Technical requirements

There are several requirements for the envisioned applications. First, we expect a spatial resolution of the order of hundreds of µm with highly contrasted images. Secondly, the γ-to-neutron suppression is expected to be above 10^6. In fact, when neutrons interact with the B_4C converter, there is a production of large fragments of α and Li particles. These fragments induce much stronger ionization of the gas compared to electrons issued from γ particles, which implies highly separated signals from the background [6]. Finally, the device will be capable of real-time radiography under two operation modes: integrated and event-by-event modes.

4.2.2. First neutron images

Recent measurements made at CERN show the first α and Li tracks captured by the optical readout glass Micromegas in event-by-event mode. Here we chose a 10.5 mm drift gap to capture long α and Li tracks. The amplification voltage is at 570V, close to the sparking limit, for a 128 µm gap. In this conditions, discharges begin to occur very rarely and have no damage effect on the ITO layer. The source is an Americium – Beryllium source, which generates 1-14 MeV neutrons with very low rate. The Fig. 12 middle represents a 5s exposure time frame where we see that the tracks are well separated from the background. The future analysis of these tracks will give precious pieces of information on the detector SNR and the analysis of the Bragg peak will lead to a reconstruction of the position of the interaction point of the neutron with the boron converter.

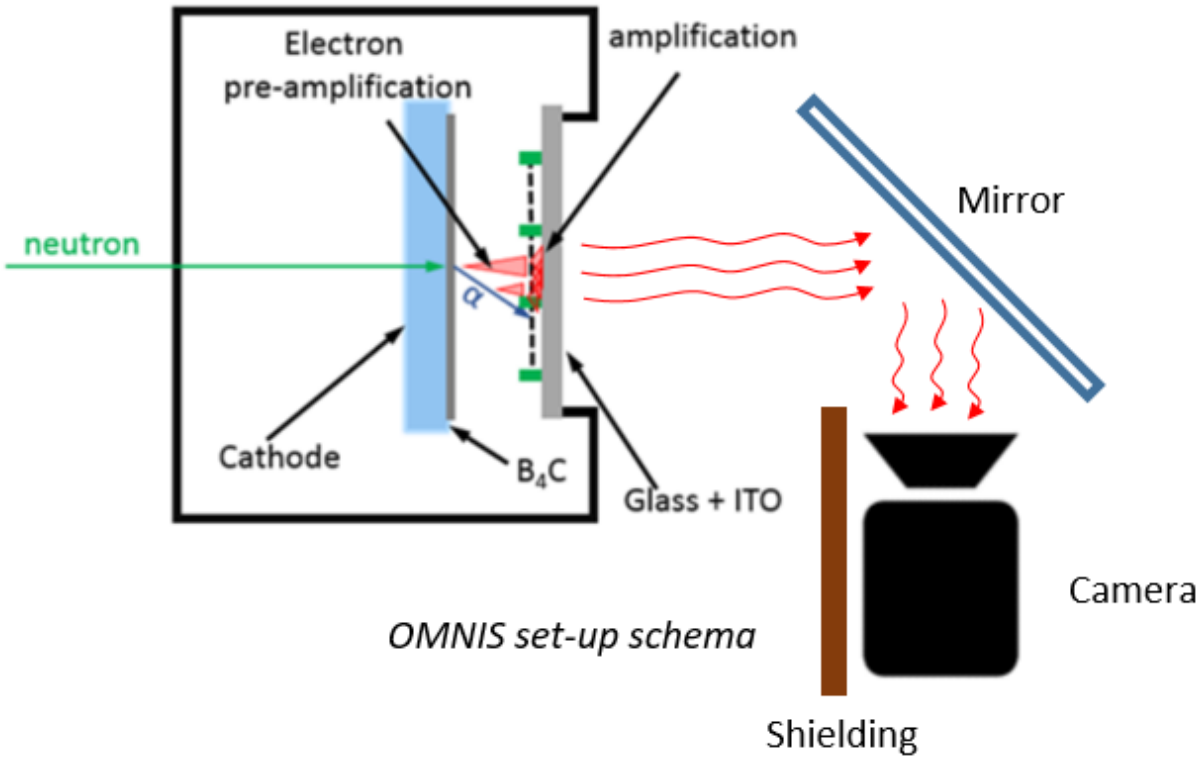

Fig. 11. Sketch of the OMNIS setup. There is a boron converter next to the cathode to convert neutrons to charges. The mirror reflects the visible light from the glass Micromegas to the camera to keep the camera safe from the high particle flux.

The optimization of the transverse diffusion in the gas is crucial. After the charged particles gas ionization, the electrons drift towards the mesh, forming an electron cloud. The cloud spreads transversally to the field direction. The cloud width at the level of the anode depends on the gas mixture, the amplification field and the amplification gap at atmospheric pressure. This effect is clearly visible when looking at highly ionizing α and Li tracks. Fig. 12 middle shows narrows tracks where the drift field is around 800 V cm^{-1}, which corresponds to the lowest transverse diffusion region on Fig. 13. In contrast, Fig. 12 left and right show thick tracks at 50 V cm^{-1} and 2000 V cm^{-1} respectively where the transverse diffusion is much higher on Fig. 13.

Nevertheless, further investigations are required on the integration method for real-time imaging. Long α and Li tracks also represent the main challenge for real-time imaging since they significantly limit the spatial resolution when integrating the tracks. One solution is to reduce the drift gap as much as possible, to minimize the track length. Even performing pre-amplification in the drift gap by implementing a few hundreds µm gap should highlight the neutron interaction point and increase the spatial resolution.

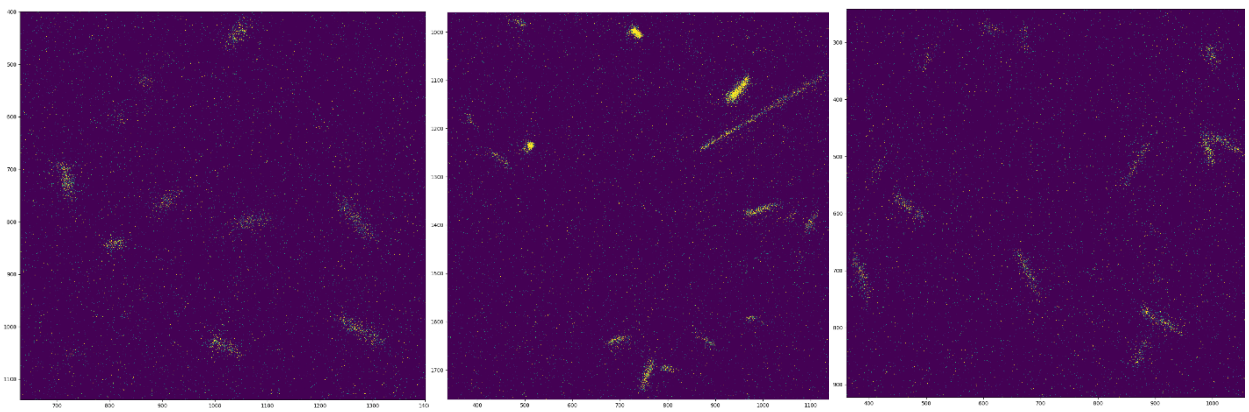

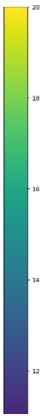

Fig. 12. Light intensity images in event-by-event mode. 5 sec exposure time images with simple background subtraction. There is 570 V in the amplification gap for a 128 µm gap and 10.5 mm drift gap. Left: 50 V drift voltage. Middle: 800 V drift voltage. Right: 2000 V drift voltage.

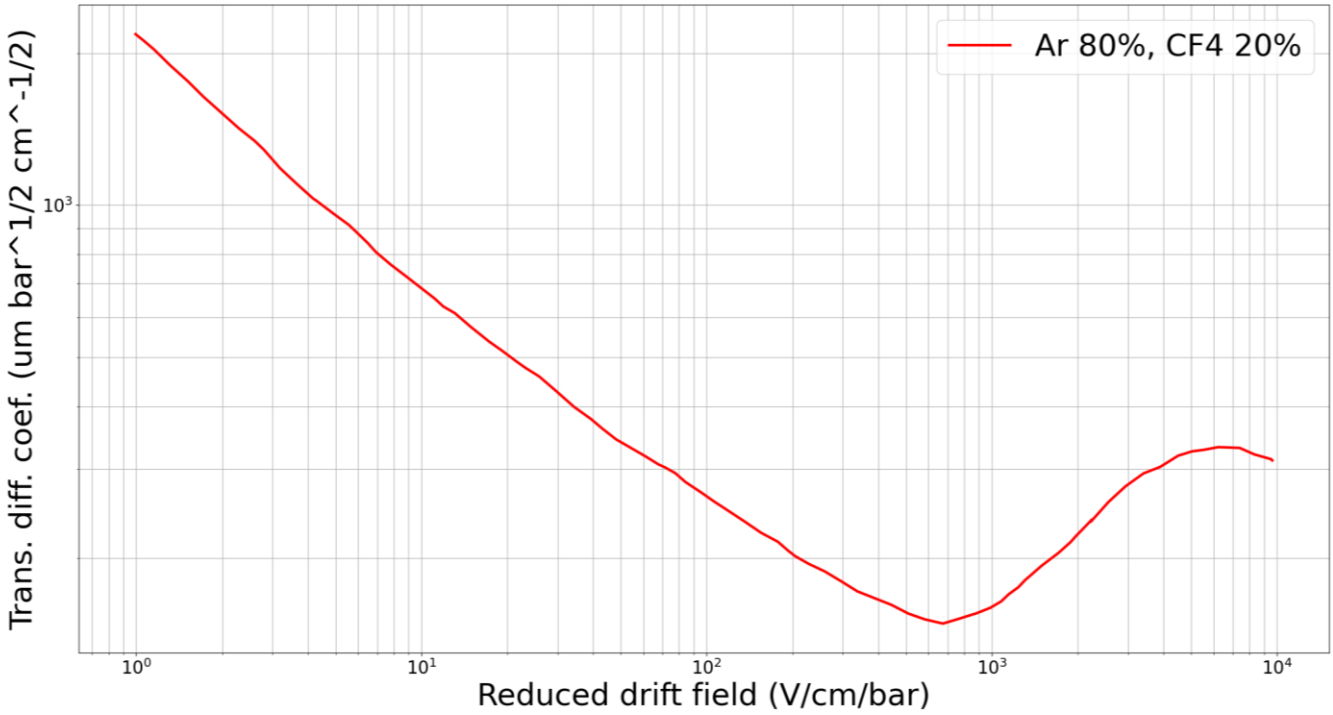

Fig. 13. Transverse diffusion in 80% Argon + 20% CF4 gas mixture.

4. Conclusion

Several prototypes of a glass Micromegas were built by integrating a Micromegas detector on a glass anode coated with ITO. The detector was tested and characterized under several types of sources and conditions. X-ray characterizations of the device were performed in integration mode for gain, contrast and spatial resolution measurements. The radiography images showed important contrast and promising resolution with almost no data analysis, thus demonstrating the potential of the integration mode for imaging. Different methods will be investigate regarding the fabrication process of the glass bulk Micromegas in order to reach better gain and stability of the detector.

Two applications are being explored for this detector: β-imaging and neutron radiography. A β-imaging prototype has been built and it performed the detection of sub-becquerel activity ^{3}H-glucose samples. Two methods were applied: the integration method showed real-time detection of 60 Bq and 0.3 Bq samples with some difficulties for the low activity drops. In event-by-event mode, highly contrasted and spatially resolved images were acquired. Measurement will be done on tritiated cells samples.

First α and Li tracks were acquired with a neutron imaging prototype. Highly contrasted tracks were acquired. The analysis of event-by-event data is in progress and is necessary to understand the influence of the diffusion in the gas on the spatial resolution. A higher neutron flux source will be used for spatial resolution measurements of the neutron imager in integration mode.

Acknowledgment

The authors acknowledge the financial support of the Cross-Disciplinary Program on Instrumentation and Detection of CEA of the French Alternative Energies and Atomic Energy Commission (CEA), of the « P2IO LabEx (ANR-10-LABX-0038)» in the framework "Investissements d'Avenir" (ANR-11-IDEX-0003-01) managed by the Agence Nationale de la Recherche (ANR), France and of the of the P2I Department of Paris-Saclay University.

References

[1] D. Attié et al, Current Status and Future Developments of Micromegas Detectors for Physics and Applications Appl.Sciences 11 (2021) 12, 5362

[2] E. Baracchini *et al,* CYGNO: a gaseous TPC with optical readout for dark matter directional search, 2020 *JINST* 15 C07036.

[3] Florian Maximilian Brunbauer thesis, Applications of gas scintillation properties in optically read out GEM-based detectors. https://cds.cern.ch/record/2632476?ln=fr

[4] F.M. Brunbauer, D. Desforge, E. Ferrer-Ribas, F.J. Iguaz, B. Mehl, R. De Oliveira, E. Oliveri, T. Papaevangelou, O. Pizzirusso, E.C. Pollacco, F. Resnati, L. Ropelewski, L. Segui, M. van Stenis, Radiation imaging with glass Micromegas, Nucl.Instrum.Meth.A 955 (2020) 163320 https://doi.org/10.1016/j.nima.2019.163320

[5] E. Seravalli. A Scintillating GEM Detector for 2D Dose Imaging in Hadron Therapy. PhD thesis, Technische Universiteit Delft, 2008. http://resolver.tudelft.nl/uuid:4035715d-a6d6-4bd3-9eb5-79e8dd99744a

[6] L. Segui et al., Characterization and First Beam Loss Detection with One ESS-nBLM System Detector. In Proceedings of the International Beam Instrumentation Conference, IBIC'19, Malmo, Sweden, 8–12 September 2019; JACoW Publishing: Geneva, Switzerland, 2019; pp. 29–35., https://doi.org/10.18429/JACoW-IBIC2019-MOBO04.

[7] A. Marusyk, V. Almendro, K. Polyak, ntra-tumour heterogeneity: a looking glass for cancer? Nat. Rev. Cancer 12 (2012) 323–334, http://dx.doi.org/10.1038/ nrc3261.

[8] F. Jambon et al. Medica-Plus: a novel Micromegas detector for high-resolution \betaβ imaging for improved pharmacological applications, J.Phys.Conf.Ser. 1498 (2020) 1, 012046

[9] A. Pansky et al. The scintillation of CF4 and its relevance to detection science. Nucl. Instruments Methods Phys. Res. Sect. A, 354(2-3):262–269, 1995.

[10] Hamamatsu,SCAS0152E_ORCA-Quest_concept_brochure, https://www.hamamatsu.com/content/dam/hamamatsu-photonics/sites/documents/99_SALES_LIBRARY/sys/SCAS0152E_ORCA-Quest_concept_brochure.pdf

[11] F. Jambon, S. Aune, P. Baron, T. Benoit, T. Bey, D. Desforge, E. Ferrer-Ribas, A. Grabas, M. Kebbiri, I. Mandjavidze, T. Papaevangelou, M. Riallot, M. Vandenbroucke, F. Beau, V. Dive, C. Malgorn, F. Malloggi, A. Rousselot, F. Carrel, M. Trocmé, Medica-Plus: A Micromegas-based proof-of-concept detector for sub-becquerel tritium activity assessment at the service of oncological research, Nuclear Inst. and Methods in Physics Research, A, Volume 1027, article id. 166332. March 2022